Journal of Materials Chemistry A

Accepted Manuscript

ROYAL SOCIETY OF CHEMISTRY

www.rsc.org/materialsA

Journal Name

ARTICLE

Core-shell $Co_3O_4/ZnCo_2O_4$ coconut-like hollow spheres with extremely high performance as anode materials for lithium-ion batteries

Received 00th January 20xx,
Accepted 00th January 20xx

DOI: 10.1039/x0xx00000x

www.rsc.org/

Qiang Wang, Binwei Yu, Xiao Li, Lili Xing* and Xinyu Xue*

Core-shell $Co_3O_4/ZnCo_2O_4$ coconut-like hollow spheres are synthesized by a facile two-step method. As the anode of lithium-ion batteries, their reversible capacity is up to 1278 mAh g^{-1} at 0.1C rate and keeps at 1093 mAh g^{-1} after 50 cycles, much higher than that of pure Co_3O_4. Even after 300 cycles (cycling for more than 4 months), their reversible capacity can maintain at 934 mAh g^{-1} at 0.2C rate. Such superior electrochemical performance (high reversible capacity, excellent long-term cycling stability and good rate capability) can be ascribed to the unique core-shell hollow structure, complex synergistic effect, good electrical conductivity and interfacial charging mechanism. The present results demonstrate that the core-shell $Co_3O_4/ZnCo_2O_4$ hollow spheres are promising anode materials for high-performance lithium-ion batteries.

Introduction

Rechargeable lithium-ion batteries (LIBs) have been regarded as an excellent power source for portable electronics due to their advantages of high energy density, no memory effect, long lifespan, little self-discharge and environmental benignity.[1-6] Recently, various transition metal oxides as promising alternatives to the commercial graphite anode have attracted much attention because of their high theoretical capacity and energy density.[4-13] Among these transition metal oxides, cobalt oxide (Co_3O_4) is one of the most widely studied materials due to its high theoretical capacity of 890 mAh g^{-1} (about two times higher than 372 mAh g^{-1} of commercial graphite).[14-21] However, as anodes for LIBs, the poor cycling stability and low rate capability of Co_3O_4 materials (arising from poor electrical conductivity and large volume expansion) restrain their practical application.[22-26]

Some effective strategies have been proposed to solve these problems, such as preparing low-dimensional nanostructures, coating carbon on the surface and fabricating hollow structures.[25-28] For example, Lou et. al. reported that the hollow structures can provide large interfacial contact area and short lithium transport distance, leading to high rate capabilities; meanwhile, the void space in the hollow nanostructures can also buffer the huge volume changes of the material and alleviate the pulverization, leading to good cycling stability.[26-28] Nowadays, much research effort has also been made to investigate the ternary metal oxides materials as the anode of LIBs for their complementary behavior and synergistic effect between the two metal elements, such as $CoMn_2O_4$, $ZnCo_2O_4$, $NiCo_2O_4$ and $MnCo_2O_4$.[29-32] Among them, $ZnCo_2O_4$ anode materials have received special attention because of their unique crystalline structure and remarkable electrochemical reaction mechanism toward lithium ions.[33] In the cubic spinel $ZnCo_2O_4$ structure, the Zn^{2+} ions occupy the tetrahedral sites and the Co^{2+} ions hold the octahedral sites.[34] Since both Zn and Co have electrochemically activity to lithium, a complementary manner can contribute to the enhanced lithium-storage performance.[30,35] At the same time, such complex ternary compound can possess high electronic conductivity.[31-37] Thus, it is highly expected that core-shell $Co_3O_4/ZnCo_2O_4$ hollow-structure composites could have high storage capacity, excellent cycling stability and good rate capability due to their unique hollow structure and the complex synergistic effect.

In this work, core-shell $Co_3O_4/ZnCo_2O_4$ coconut-like hollow spheres have been fabricated by a simple two-step method, and as the anode of LIBs, superior performance with high reversible capacity, excellent long-term cycling stability and good rate capability has been achieved.

Experimental

All the chemical reagents were of analytical grade and directly used without any further purification.

Synthesis of pure Co_3O_4 hollow spheres

Pure Co_3O_4 hollow spheres were synthesized by a hydrothermal method. In a typical process, 1.324 g $Co(NO_3)_2{\cdot}6H_2O$, 0.448 g $C_6H_5Na_3O_7{\cdot}2H_2O$ and 0.321 g $C_6H_{12}N_4$ were added into 35 mL deionized water. After stirring for 20

College of Sciences, Northeastern University, Shenyang 110004, China.
E-mail: xinglili@mail.neu.edu.cn; xuexinyu@mail.neu.edu.cn;
Tel: (+86) 24-83687658.

min, the solution was kept at 100°C for 24 h in a 50 mL Teflon-lined stainless steel autoclave. After being cooled down to room temperature, the precipitates were collected by centrifugation, washed for several times with deionized water and absolute ethanol, and then dried in vacuum at 60°C for 12 h. Finally, the products were annealed at 200°C in air for 3 h.

Synthesis of core-shell $Co_3O_4/ZnCo_2O_4$ hollow spheres

Core-shell $Co_3O_4/ZnCo_2O_4$ hollow spheres were prepared via a wet-chemical route. Firstly, as-prepared Co_3O_4 hollow spheres (0.200 g) were dispersed in 20 mL deionized water under ultrasonic treatment for 30 min. Then, 0.447 g $Zn(NO_3)_2·6H_2O$ and 0.224 g $C_6H_5Na_3O_7·2H_2O$ were added to the solution. After magnetically stirring at 90°C for 12 h, the products were collected, washed with deionized water and absolute ethanol for several times, and dried in vacuum at 60°C for 12 h. Finally, the products were calcined at 400°C in air for 3 h.

Materials characterization

The crystal structures of pure Co_3O_4 and core-shell $Co_3O_4/ZnCo_2O_4$ hollow spheres were characterized by X-ray power diffraction (XRD, D/max 2550V, CuK_α Radiation, λ=1.5416 Å) in 2θ range from 10° to 90°. The morphology and microstructure of the samples were examined using scanning electron microscope (SEM, Hitachi S4800) with an energy dispersive X-ray spectrometer (EDX) and transmission electron microscope (TEM, JEOL JEM-2010), respectively.

Electrochemical measurement

The working electrodes were prepared by mixing active material, conductive graphite and carboxymethyl cellulose (CMC) with a mass ratio of 80:10:10. The mixture was painted onto copper foils with a diameter of 15 mm, and dried at 100°C under vacuum for 12 h. The liquid electrolyte was composed of 1 mol L^{-1} $LiPF_6$ in the mixture of 50 vol% ethylene carbonate (EC) and 50 vol% dimethyl carbonate (DMC). Standard 2016 coin-type cells were assembled in an argon filled glove box. Pure lithium foils were used as the counter electrodes. The galvanostatic charge/discharge tests were carried out in the voltage range of 0.001 to 3.000 V versus Li^+/Li under room temperature at various current rates.

Results and discussion

Fig. 1 shows the XRD patterns of pure Co_3O_4, pure $ZnCo_2O_4$ and core-shell $Co_3O_4/ZnCo_2O_4$ hollow spheres. In curve a, all the diffraction peaks can be indexed to cubic spinel Co_3O_4 crystal with a space group of *Fd3m* (JCPDS card No. 42-1467). The diffraction peaks in curve b can be well indexed to the cubic $ZnCo_2O_4$ phase (JCPDS card No. 23-1390). The diffraction peaks in curve c can be indexed to Co_3O_4 and $ZnCo_2O_4$ phases, and no additional diffraction peaks from other impurities can be observed, indicating that the as-synthesized core-shell $Co_3O_4/ZnCo_2O_4$ hollow spheres have high phase purity.

The morphology and structure of pure Co_3O_4 hollow spheres are shown in Fig. 2. The typical SEM images of pure Co_3O_4 hollow spheres (Fig. 2a-c) show that the surface of pure Co_3O_4

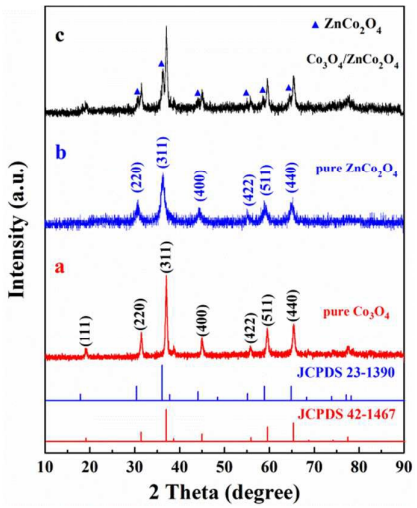

Fig. 1 XRD diffraction patterns of (a) pure Co_3O_4, (b) pure $ZnCo_2O_4$ and (c) core-shell $Co_3O_4/ZnCo_2O_4$ hollow spheres.

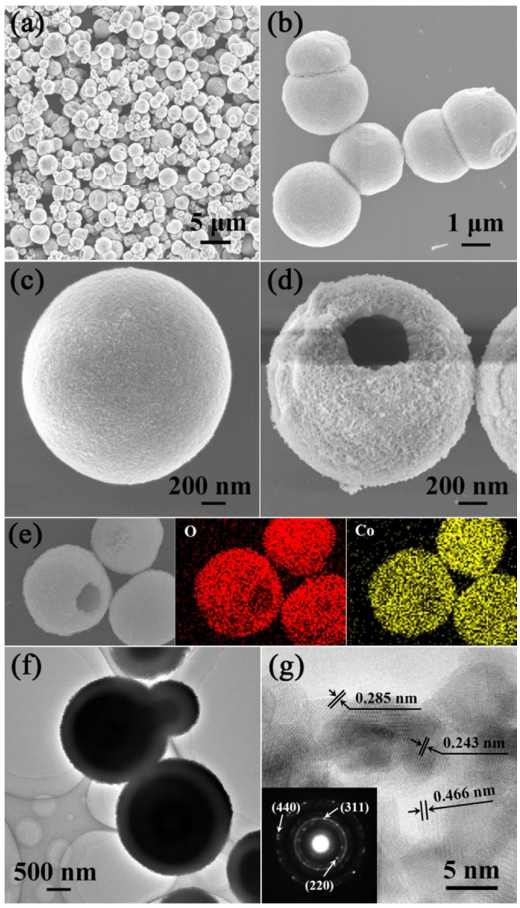

Fig. 2 (a, b, c, d) SEM, (e) elemental mapping and (f) TEM images of pure Co_3O_4 hollow spheres. (g) HRTEM image of pure Co_3O_4 hollow sphere. Inset: selected area electron diffraction (SAED) pattern.

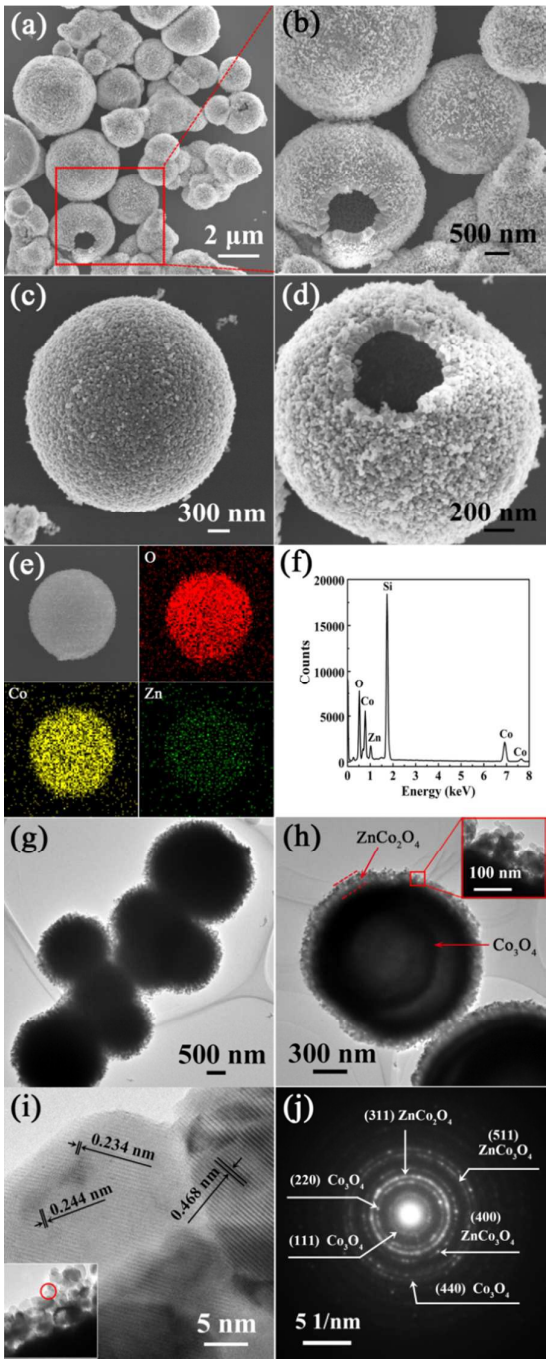

Fig. 3 (a-d) SEM images, (e) elemental mapping, (f) EDX spectrum, (g, h) TEM images, (i) HRTEM image and (j) SAED pattern of core-shell $Co_3O_4/ZnCo_2O_4$ hollow spheres.

hollow spheres is smooth and the diameter is in the range of 1~3 μm. From Fig. 2d, the hollow structure can be clearly observed from the broken sphere. The element mapping results (Fig. 2e) indicate the uniform distribution of O and Co elements in the composite. The typical TEM image of pure Co_3O_4 hollow spheres is presented in Fig. 2f, confirming the spherical structure. Fig. 2g is high resolution TEM (HRTEM) image of a Co_3O_4 hollow sphere. The crystal lattice fringes of 0.243, 0.285 and 0.466 nm agree well with (311), (220) and (111) planes of cubic spinel Co_3O_4 crystal, respectively. The inset of Fig. 2g is the corresponding selected area electron diffraction (SAED) pattern.

The SEM images of core-shell $Co_3O_4/ZnCo_2O_4$ coconut-like hollow spheres are displayed in Fig. 3a and 3b. The diameter of core-shell $Co_3O_4/ZnCo_2O_4$ hollow spheres ranges from 1.2 to 3.5 μm. The high-magnification SEM images of a single (Fig. 3c) and a broken (Fig. 3d) core-shell $Co_3O_4/ZnCo_2O_4$ hollow spheres show that the whole surface of Co_3O_4 hollow spheres are uniformly coated with $ZnCo_2O_4$ nanoparticles. The elemental mapping results and EDX spectrum of a core–shell $Co_3O_4/ZnCo_2O_4$ hollow sphere are shown in Fig. 3e and 3f, respectively. The O, Co and Zn elements are uniformly distributed along the sphere, indicating that the whole surface of Co_3O_4 hollow spheres are coated with $ZnCo_2O_4$ nanoparticles. The EDX spectrum also reveals that the final product consists of the three elements. From the typical TEM images of core-shell $Co_3O_4/ZnCo_2O_4$ hollow spheres (Fig. 3g and 3h), it can be clearly seen that a large amount of $ZnCo_2O_4$ particles are uniformly distributed on the whole surface of Co_3O_4 spheres. The hollow space is about 52% of total volume of the sphere. Fig. 3i is the HRTEM image of the selected areas. The crystal lattice fringes of 0.468, 0.244 and 0.234 nm agree well with the spacing of (111), (311) and (222) planes of cubic $ZnCo_2O_4$ crystal, respectively. The SAED pattern of core-shell $Co_3O_4/ZnCo_2O_4$ hollow spheres is shown in Fig. 3j. The two different crystal natures can be indexed to cubic spinel Co_3O_4 and cubic $ZnCo_2O_4$ phases, respectively.

The growth mechanism of core-shell $Co_3O_4/ZnCo_2O_4$ hollow spheres is schematically illustrated in Fig. 4. At the initial stage, during the hydrothermal process, $C_6H_{12}N_4$ generates many formaldehyde (HCHO) gas bubbles and slowly releases OH^- ions through thermal treatment ($C_6H_{12}N_4 + 6H_2O \rightarrow 6HCHO(gas) + 4NH_3$, $NH_3 + H_2O \rightarrow NH_4^+ + OH^-$).[39-41] Then, $Co(NO_3)_2{\cdot}6H_2O$ is used as the source of Co^{2+} ions, and Co^{2+} ions react with OH^- ions to form $Co(OH)_2$ nanoparticles in solution ($Co^{2+} + 2OH^- \rightarrow Co(OH)_2$).[16,43,44] Consequently, the $Co(OH)_2$ nanoparticles tend to attach on the surface of HCHO gas bubbles. With the reaction time prolonging, lots of $Co(OH)_2$

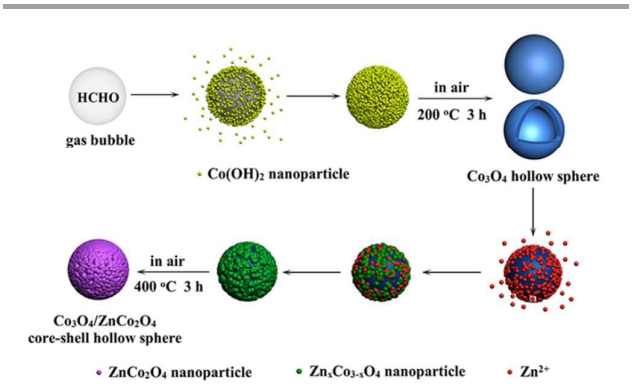

Fig. 4 Schematic illustrations of the growth mechanism for core-shell $Co_3O_4/ZnCo_2O_4$ hollow spheres.

nanoparticles aggregate around the gas bubble surface. This process continues until the formation of hollow spheres. And Co_3O_4 hollow spheres are formed after annealing in air ($6Co(OH)_2 + O_2 \rightarrow 2Co_3O_4 + 6H_2O$).[16,44] After $Zn(NO_3)_2{\cdot}6H_2O$ is added to the solution containing as-synthesized Co_3O_4 hollow spheres, many Zn^{2+} ions can be absorbed on the surfaces of Co_3O_4 hollow spheres. Then these Zn^{2+} ions can react with Co_3O_4, resulting in the formation of $Zn_xCo_{3-x}O_4$ nanoparticles on the surface.[33,45,46] With the reaction time prolonging, more and more $Zn_xCo_{3-x}O_4$ nanoparticles are formed on the surface to build a shell of $Zn_xCo_{3-x}O_4$. Finally, core-shell $Co_3O_4/ZnCo_2O_4$ hollow spheres are obtained after annealing in air at 400°C.

The electrochemical performances of pure Co_3O_4 and core-shell $Co_3O_4/ZnCo_2O_4$ hollow spheres are shown in Fig.5. Fig. 5a shows the discharge/charge capacities versus the voltage of $Co_3O_4/ZnCo_2O_4$ hollow spheres at 0.1C rate (10 hours per half cycle). A clear potential plateau at ~0.98 V is observed for 1st cycle in the discharge curve. And the discharge potential plateau shifts to ~1.07 V for the subsequent cycles. The initial discharge/charge capacities of core-shell $Co_3O_4/ZnCo_2O_4$ hollow spheres are 1831/1186 mAh g^{-1} with a large irreversible capacity loss of 645 mAh g^{-1} and a low coulombic efficiency of 65%. The large capacity loss can be ascribed to the formation of solid electrolyte interphase (SEI) layer, the inactivation of some inserted Li-ion and the reduction of electrolyte.[43-49] The discharge/charge capacities of 2nd, 10th, 30th and 50th cycles are 1278/1233, 1130/1109, 1144/1132 and 1093/1090 mAh g^{-1}, respectively. Fig. 5b shows the cycling performances of pure Co_3O_4 and core–shell $Co_3O_4/ZnCo_2O_4$ hollow spheres at 0.1C rate for 50 cycles. For pure Co_3O_4 hollow spheres, the reversible discharge capacity (the second discharge capacity) is 856 mAh g^{-1}, and its discharge capacity reduces rapidly to 435 mAh g^{-1} after 50 cycles with low capacity retention of 51%. For core–shell $Co_3O_4/ZnCo_2O_4$ hollow spheres, the reversible discharge capacity is 1278 mAh g^{-1}, much higher than the theoretical capacities of Co_3O_4 (~890 mAh g^{-1})[27] and $ZnCo_2O_4$ (~900 mAh g^{-1}).[33-35] After 50 cycles, the discharge capacity keeps at 1093 mAh g^{-1} with high capacity retention of 86%.

Fig. 5c and 5d are the cycling performances of pure Co_3O_4 and core-shell $Co_3O_4/ZnCo_2O_4$ hollow spheres during 50 cycles at different current rates, respectively. For pure Co_3O_4 hollow spheres, after 50 cycles, the discharge capacities rapidly decrease to 435, 421, 330, 257 and 182 mAh g^{-1} at 0.1C, 0.2C, 0.3C, 0.5C and 1C rates, respectively. The core-shell $Co_3O_4/ZnCo_2O_4$ hollow spheres (Fig. 5d) can deliver the discharge capacities of 1093, 1024, 965, 805 and 598 mAh g^{-1} at 0.1C, 0.2C, 0.3C, 0.5C and 1C rates after 50 cycles, respectively. Furthermore, long-term cycling performance of core-shell $Co_3O_4/ZnCo_2O_4$ hollow spheres is investigated at 0.2C, 0.3C and 0.5C rates for 300 cycles as shown in Fig. 5e. After 300 cycles (cycling for more than 4 months), the reversible capacities of core-shell $Co_3O_4/ZnCo_2O_4$ hollow spheres can still reach 934, 784 and 697 mAh g^{-1} with the capacity retentions of 78%, 68% and 81% at 0.2C, 0.3C and 0.5C rates, respectively. The discharge capacity keep constant from 20th cycle to 300th cycle and the capacity retentions are 96%, 90% and 91% at 0.2C, 0.3C and 0.5C rates, respectively.

The rate capabilities of pure Co_3O_4 and core-shell $Co_3O_4/ZnCo_2O_4$ hollow spheres are shown in Fig. 5f. The discharge capacities of pure Co_3O_4 hollow spheres are 869, 802, 682, 595, 397 and 192 mAh g^{-1} at 0.1C, 0.2C, 0.3C, 0.5C, 1C and 2C rates, respectively. When the rate returns to 0.2C and 0.1C, the capacities recover to merely 490 and 519 mAh g^{-1}, respectively. For core-shell $Co_3O_4/ZnCo_2O_4$ hollow spheres, the discharge capacities are 1238, 1056, 959, 845, 770 and 644 mAh g^{-1} at 0.1C, 0.2C, 0.3C, 0.5C, 1C and 2C rates, respectively. After the rate return to 0.2C and 0.1C, the capacities recover to 1059 and 1131 mAh g^{-1}, respectively. Compared with pure Co_3O_4 hollow spheres, the core-shell $Co_3O_4/ZnCo_2O_4$ hollow spheres exhibit higher capacity and better cycling performance.

The conductivities of pure Co_3O_4 and $Co_3O_4/ZnCo_2O_4$ electrodes are investigated by electrochemical impedance spectroscopy (EIS) measurements after 10 cycles at 0.1C rate. Fig. 5g gives the Nyquist plots for the two electrodes. The inset of Fig. 5g is the equivalent electrical circuit, which includes the ohmic resistance R_Ω, the Faradic charge transfer resistance R_{ct}, the Warburg impedance W and the double layer capacitance CPE.[50] The Nyquist plots consist of a semicircle in the high-to-medium frequency region and a sloping long line in the low-frequency region, which are attributed to the charge-transfer process and the mass transfer of lithium ions, respectively.[50,51] Obviously, the semicircle diameter of $Co_3O_4/ZnCo_2O_4$ electrode is smaller than that of pure Co_3O_4 electrode, indicating that $Co_3O_4/ZnCo_2O_4$ electrode possesses a more stable surface film (including the SEI layer) and faster charge-transfer at the electrode/electrolyte interface than pure Co_3O_4 electrode.[33]

Table 1 shows the comparison of the electrochemical performances between core-shell $Co_3O_4/ZnCo_2O_4$ hollow spheres and other previously results (Co_3O_4- or $ZnCo_2O_4$-based nanocomposites). It can be seen that the core-shell $Co_3O_4/ZnCo_2O_4$ hollow spheres exhibit good long-term cycling stability.

To further understand the electrochemical behavior during discharge/charge process, the XRD measurements of pure Co_3O_4 and $Co_3O_4/ZnCo_2O_4$ electrodes are carried out after 10 cycles at 0.1C rate, as shown in Fig. 6. In the XRD patterns, the peaks of Cu and C arise from copper foil and conductive graphite. For pure Co_3O_4 hollow spheres, after discharge process (Fig. 6a), the diffraction peaks can be indexed to Li_2O (JPCDS File No. 12-0254) and Co (JPCDS File No. 65-9722). After charge process (Fig. 6b), the diffraction peaks of Co_3O_4 (JPCDS File No. 42-1467) and CoO (JPCDS File No. 42-1300) can be observed. For core-shell $Co_3O_4/ZnCo_2O_4$ hollow spheres, after discharge process (Fig. 6c), the diffraction peaks can be indexed to Li_2O (JPCDS File No. 12-0254), Co (JPCDS File No. 65-9722), Zn (JPCDS File No. 04-0831) and LiZn (JPCDS File No. 03-0954). After charge process (Fig. 6d), the diffraction peaks of Co_3O_4 (JPCDS File No. 42-1467), CoO (JPCDS File No. 42-1300), ZnO (JPCDS File No. 36-1451) and Zn (JPCDS File No. 04-0831) are observed. No peaks of Li_2O can be observed, indicating that almost all of Li_2O reversibly convert into Li^+.

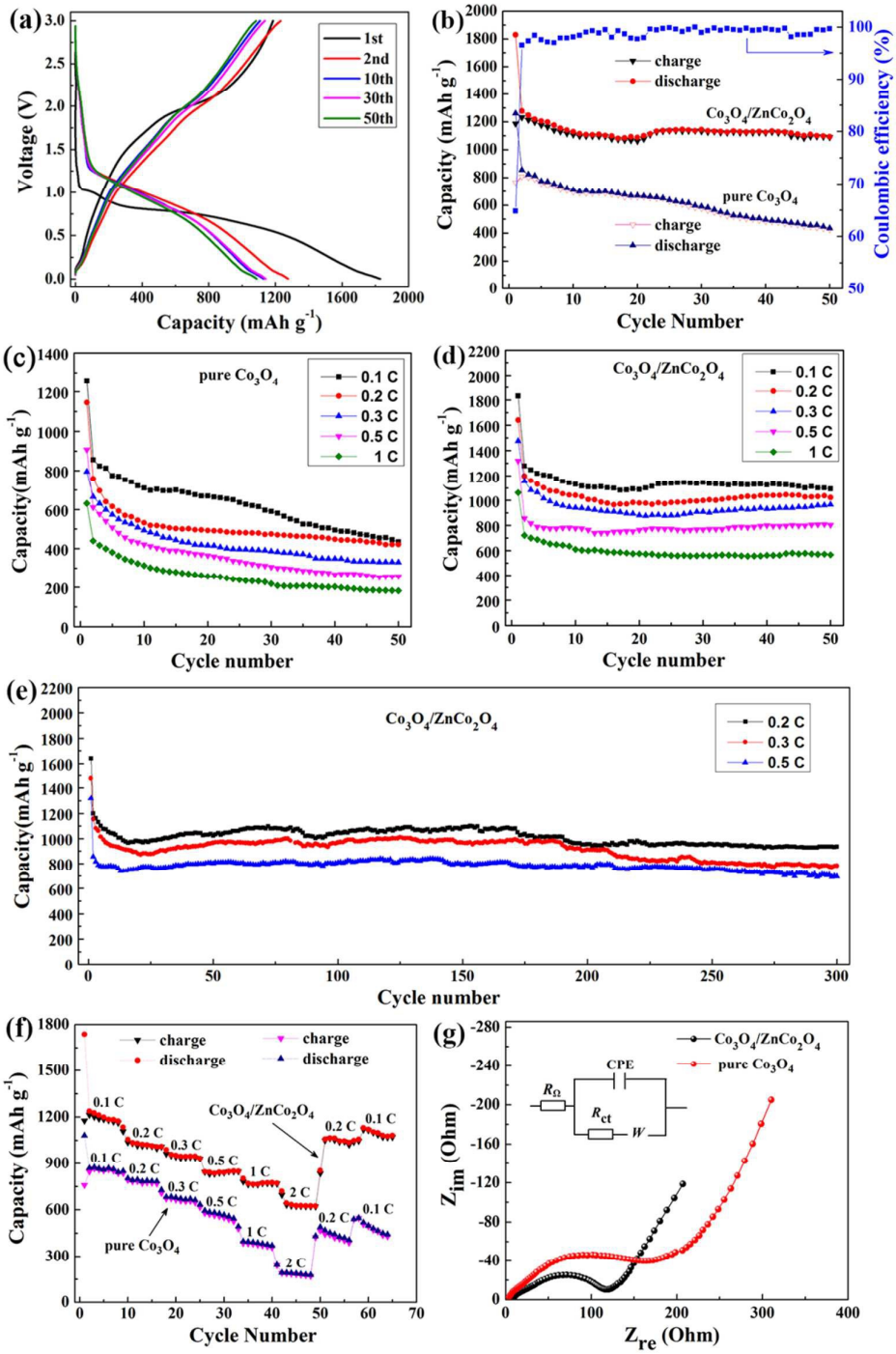

Fig. 5 (a) The discharge/charge voltage profiles of $Co_3O_4/ZnCo_2O_4$ at 0.1 rate. (b) The cycling performance and coulombic efficiency of $Co_3O_4/ZnCo_2O_4$ at 0.1C rate. The cycling performances of (c) pure Co_3O_4 and (d) $Co_3O_4/ZnCo_2O_4$ hollow spheres at 0.1C, 0.2C, 0.3C, 0.5C and 1C rates. (e) The cycling performance of $Co_3O_4/ZnCo_2O_4$ for 300 cycles at 0.2C, 0.3C and 0.5C rates. (f) The rate capabilities of pure Co_3O_4 and $Co_3O_4/ZnCo_2O_4$ at various current rates. (g) The Nyquist plots of pure Co_3O_4 and $Co_3O_4/ZnCo_2O_4$ electrodes after 10 cycles at 0.1C rate.

Table 1 Comparison of electrochemical performances between core-shell $Co_3O_4/ZnCo_2O_4$ hollow spheres and other previously results.

Electrode material	Capacity	Current density	Cycles	References
$Co_3O_4/ZnCo_2O_4$	1051 mAh g^{-1}	0.2C (230 mA·g^{-1})	100	This work
	934 mAh g^{-1}	0.2C (230 mA·g^{-1})	300	This work
Co_3O_4 hexapods	800 mAh g^{-1}	100 mA·g^{-1}	40	[6]
Co_3O_4 hollow spheres	866 mAh g^{-1}	178 mA·g^{-1}	50	[17]
Co_3O_4 flowers	694 mAh g^{-1}	100 mA·g^{-1}	100	[24]
Co_3O_4/onion-like carbon	632 mAh g^{-1}	200 mA·g^{-1}	100	[22]
Double-shelled Co_3O_4	1303 mAh g^{-1}	50 mA·g^{-1}	30	[52]
Co_3O_4 nanoflakes	806 mAh g^{-1}	0.1C	300	[53]
SnO_2@Co_3O_4 spheres	962 mAh g^{-1}	100 mA·g^{-1}	100	[54]
$ZnCo_2O_4$ hollow powders	586 mAh g^{-1}	3000 mA·g^{-1}	200	[55]
Mesoporous $ZnCo_2O_4$	721 mAh g^{-1}	100 mA·g^{-1}	80	[36]
$ZnCo_2O_4$ nanoflakes	750 mAh g^{-1}	80 mA·g^{-1}	50	[61]
$ZnCo_2O_4$ nanowires	890 mAh g^{-1}	200 mA·g^{-1}	50	[56]
$ZnxCo_{3-x}O_4$ dodecahedra	990 mAh g^{-1}	100 mA·g^{-1}	50	[57]
$ZnCo_2O_4$ twin spheres	831.7 mAh g^{-1}	1000 mA·g^{-1}	100	[58]
$ZnCo_2O_4$ /carbon cloth	1200 mAh g^{-1}	200 mA·g^{-1}	160	[59]

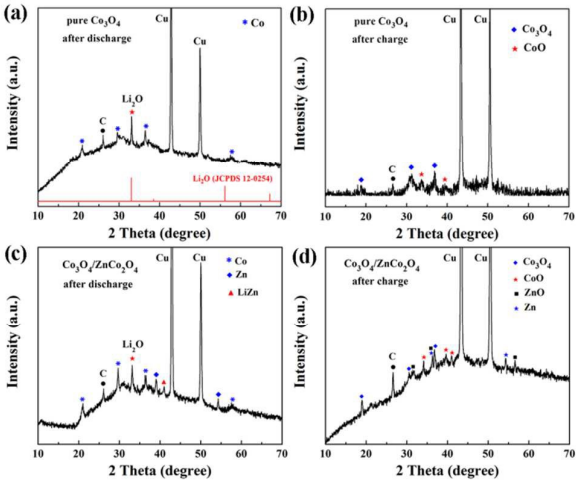

Fig. 6 XRD patterns of (a, b) pure Co_3O_4 and (c, d) core-shell $Co_3O_4/ZnCo_2O_4$ hollow spheres electrodes after 10 cycles at 0.1C rate.

The differential capacity curves (dC/dV vs. potential) of pure Co_3O_4, pure $ZnCo_2O_4$ and $Co_3O_4/ZnCo_2O_4$ electrodes are investigated in the voltage range from 0.001 to 3.000 V. Fig. 7a is the differential capacity curves of pure Co_3O_4 electrode for 1st, 2nd, 10th, 30th and 50th cycles. In the first discharge (Li insertion) process, an irreversible peak at 0.92 V is observed, which can be attributed to the conversion from Co_3O_4 to intermediate-phase CoO, and then to metallic Co with the formation of SEI films.[23,60] In the subsequent processes, the reduction peak is shifted to 1.04 V, which corresponds to the reduction reactions of CoO and Co_3O_4 to metallic Co.[21,60] During the charge (Li extraction) processes, a main broad oxidation peak around 2.01 V is observed, which can be ascribed to the multistep oxidation reactions of Co to CoO and

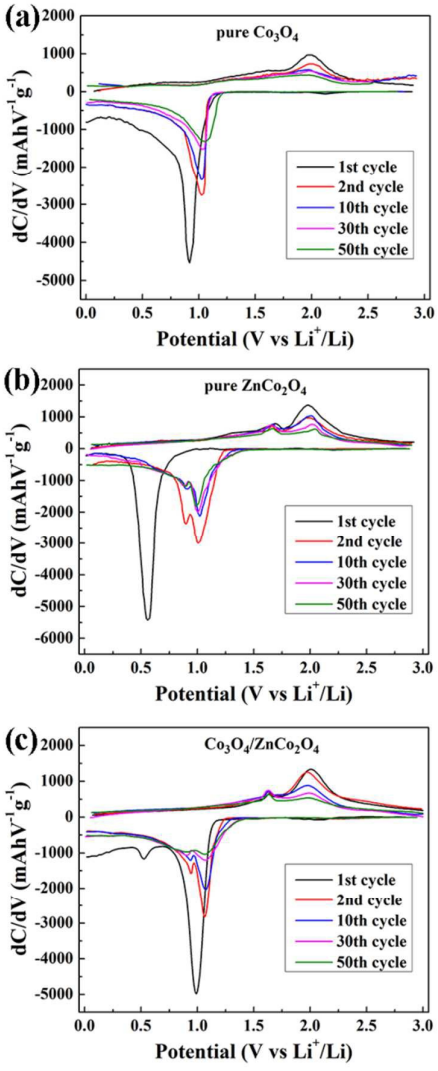

Fig. 7 The differential capacity curves (dC/dV vs. potential) of (a) pure Co_3O_4, (b) pure $ZnCo_2O_4$ and (c) core-shell $Co_3O_4/ZnCo_2O_4$ hollow spheres for the 1st, 2nd, 10th, 30th and 50th cycles.

Co_3O_4. The electrochemical reactions are presented as follows:[21,23,60]

$$Co_3O_4 + 8Li^+ + 8e^- \leftrightarrow 3Co + 4Li_2O \quad (1)$$

$$CoO + 2Li^+ + 2e^- \leftrightarrow Co + Li_2O \quad (2)$$

Fig. 7b shows the differential capacity curves of pure $ZnCo_2O_4$ electrode. In the first discharge process, an irreversible reduction peak located at 0.56 V is observed, which can be assigned to the reduction of $ZnCo_2O_4$ to Zn and Co with the formation of SEI films.[33,61] In the following discharge processes, two reduction peaks at 1.02 V and 0.91 V can be observed. The peak at 1.02 V can be attributed to the reduction of ZnO and CoO/Co_3O_4, and the peak at 0.91 V is probably due to alloying reaction of Li-Zn.[60-62] Two oxidation peaks located at 1.67 V

and 2.02 V are observed during the charge processes. The peak at 1.67 V probably corresponds to the dealloying process of Li-Zn and the broad peak at 2.02 V can be attributed to the oxidation of Zn and Co.[60-62] Fig. 7c is the differential capacity curves of core-shell $Co_3O_4/ZnCo_2O_4$ hollow spheres electrode. Two reduction peaks located at 0.98 V and 0.53 V are observed in the first discharge process. The peak at 0.98 V can be attributed to the reduction of Co_3O_4 to CoO and Co with the formation of SEI films.[23,60] The peak at 0.53 V can be attributed to the irreversible reduction of $ZnCo_2O_4$ to Zn and Co.[33,61] In the following discharge processes, it can be observed that the reduction peaks are shifted to 1.07 V and 0.94 V. The main peak at 1.07 V is probably due to the reduction of ZnO and CoO/Co_3O_4, and the weak peak at 0.94 V can be attributed to the reversible alloying reaction of Li-Zn.[60-62] During the charge processes, the peak observed at 1.63 V probably arises from the dealloying process of Li-Zn.[60-62] The broad peak around 2.01 V can be attributed to the oxidation of Zn and Co.[60-62] The lithium insertion and extraction reactions for $ZnCo_2O_4$ can be illustrated as follows: [61-63]

$$ZnCo_2O_4 + 8Li^+ + 8e^- \rightarrow Zn + 2Co + 4Li_2O \quad (3)$$

$$Zn + Li^+ + e^- \leftrightarrow LiZn \quad (4)$$

$$Zn + Li_2O \leftrightarrow ZnO + 2Li^+ + 2e^- \quad (5)$$

$$Co + Li_2O \leftrightarrow CoO + 2Li^+ + 2e^- \quad (6)$$

$$CoO + 1/3\,Li_2O \leftrightarrow 1/3\,Co_3O_4 + 2/3\,Li^+ + 2/3\,e^- \quad (7)$$

The ex-situ SEM images of core-shell $Co_3O_4/ZnCo_2O_4$ hollow spheres after 100 cycles at 0.5C rate are shown in Fig. 8. It can be seen that the samples are still mainly dominated by spherical structures after 100 cycles. After discharge process (Fig. 8a), the average diameter of spheres is about 2.23 μm, and the average diameter after charge process (Fig. 8b) is about 2.04 μm. The volume expansion rate is about 131%. These results demonstrate that core-shell $Co_3O_4/ZnCo_2O_4$ hollow structures can accommodate the strain and keep the structural integrity during cycles.

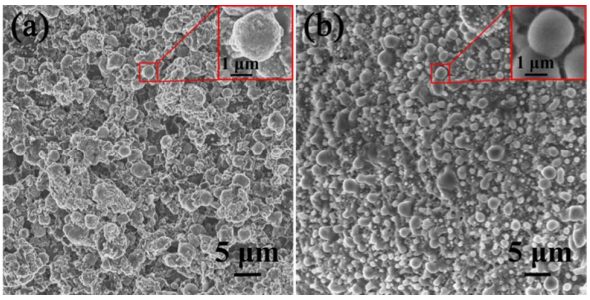

Fig. 8 Ex-situ SEM images of $Co_3O_4/ZnCo_2O_4$ core-shell hollow spheres after (a) discharge process and (b) charge process of the 100th cycle at 0.5C rate.

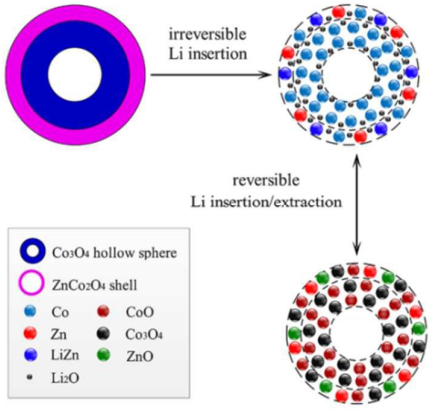

Fig. 9 Schematic illustration of the Li insertion/extraction mechanism for core-shell $Co_3O_4/ZnCo_2O_4$ hollow spheres.

Li insertion/extraction processes of $Co_3O_4/ZnCo_2O_4$ hollow spheres are schematically illustrated in Fig. 9. After the first discharge process, the materials undergo an irreversible reaction between Li^+ and $Co_3O_4/ZnCo_2O_4$ to form the nanodispersed metallic particles (Co, Zn), LiZn alloy and Li_2O. According to Eqn. 3, $ZnCo_2O_4$ can provide extra Li_2O by the initial irreversible reaction. In the following cycles, the nanodispersed metallic particles (Co, Zn) can probably make these extra Li_2O reversibly convert to Li^+, which can enhance the reversible capacity. At the same time, the extra alloying step of Zn and Li (Eqn. 4) can provide extra capacity.[13,33] On the other hand, the nanodispersed Co and Zn metal particles can enhance the electrical conductivity, resulting in high cycling performance.[61-66]

The superior electrochemical performance of core-shell $Co_3O_4/ZnCo_2O_4$ hollow spheres can be mainly associated with the following factors: (1) The core-shell hollow structures have large interfacial surface areas which can shorten diffusion distance of lithium and accommodate the huge volume changes during the cycles, resulting in good cycling stability and rate capability.[26-28,67] (2) In $ZnCo_2O_4$ shell, since both Zn and Co have electrochemically activity to lithium, they can improve the lithium-storage performance by the complementary manner and the synergistic effect.[30,35] The reversible alloying/dealloying reactions of Li-Zn can also provide extra storage capacity.[33,37,45] $ZnCo_2O_4$ can provide extra Li_2O by the irreversible initial reaction, and the nanodispersed Zn and Co metal particles can make these extra Li_2O reversibly convert to Li^+ during the subsequent cycles.[9-15] Lithium ions can be stored at the large interfacial space between the $ZnCo_2O_4$ shell and the Co_3O_4 core, leading to extra capacity.[68] (3) The enhanced cycling performance can also be attributed to good electronic conductivity of core-shell $Co_3O_4/ZnCo_2O_4$ hollow spheres. The $ZnCo_2O_4$ shells possess high electrical conductivity and can facilitate the charge transfer at the electrode/electrolyte interface.[61,69]

Conclusions

In summary, core-shell $Co_3O_4/ZnCo_2O_4$ coconut-like hollow spheres have been successfully fabricated via a simple two-step method. As anode of LIBs, core-shell $Co_3O_4/ZnCo_2O_4$ hollow spheres exhibit high reversible capacity (1198 mAh g^{-1} at 0.2C), good cycling stability (934 mAh g^{-1} after 300 cycles) and excellent rate capability. The improved performance can be attributed to the unique core-shell hollow structures, complex synergistic effect, good electrical conductivity and interfacial charging mechanism. The core-shell $Co_3O_4/ZnCo_2O_4$ hollow spheres are promising anode materials for the next-generation of high-performance LIBs.

Acknowledgements

This work was supported by the National Natural Science Foundation of China (51102041 and 11104025), the Fundamental Research Funds for the Central Universities (N120205001 and N120405010), and Program for New Century Excellent Talents in University (NCET-13-0112).

Notes and references

1 H. B. Wu, J. S. Chen, H. H. Hng and X. W. Lou, *Nanoscale*, 2012, **4**, 2526-2542.
2 W. J. Hao, S. M. Chen, Y. J. Cai, L. Zhang, Z. X. Li and S. J. Zhang, *J. Mater. Chem. A*, 2014, **2**, 13801-13804.
3 G. L. Xu, J. T. Li, L. Huang, W. F. Lin and S. G. Sun, *Nano Energy*, 2013, **2**, 394-402.
4 L. Li, R. M. Li, S. L. Gai, P. Gao, F. He, M. L. Zhang, Y. J. Chen and P. P. Yang, *J. Mater. Chem. A*, 2015, **3**, 15642-15649.
5 G. Zhou, X. C. Duan, B. Liu, Q. H. Li and T. H. Wang, *Nanoscale*, 2014, **6**, 11041-11045.
6 L. Wang, B. Liu, S. Ran, H. Huang, X. Wang, B. Liang, D. Chen and G. Z. Shen, *J. Mater. Chem.*, 2012, **22**, 23541-23546.
7 B. D. Liu, F. Yuan, B. Dierre, T. Sekiguchi, S. Zhang, Y. K. Xu and X. Jiang, *ACS Appl. Mater. Interfaces*, 2014, **6**, 14159-14166.
8 L. Yu, Z. Y. Wang, L. Zhang, H. B. Wu and X. W. Lou, *J. Mater. Chem. A*, 2013, **1**, 122-127.
9 Q. Wang, Q. Wang, D. A. Zhang, J. Sun, L. L. Xing and X. Y. Xue, *Chem. Asian J.*, 2014, **9**, 3299-3306.
10 L. Zhang, H. B. Wu, B. Liu and X. W. Lou, *Energy Environ. Sci.*, 2014, **7**, 1013-1017.
11 Q. Wang, J. Sun, Q. Wang, D. A. Zhang, L. L. Xing and X. Y. Xue, *J. Mater. Chem. A*, 2015, **3**, 5083-5091.
12 X. Y. Xue, B. He, S. Yuan, L. L. Xing, Z. H. Chen and C. H. Ma, *Nanotechnology*, 2011, **22**, 395702
13 J. S. Luo, X. H. Xia, Y. S. Luo, C. Guan, J. L. Liu, X. Y. Qi, C. F. Ng, T. Yu, H. Zhang and H. J. Fan, *Adv. Energy Mater.*, 2013, **3**, 737-743.
14 X. W. Lou, D. Deng, J. Y. Lee, J. Feng and L. A. Archer, *Adv. Mater.*, 2008, **20**, 258-262.
15 Q. Wang, D. A. Zhang, Q. Wang, J. Sun, L. L. Xing and X. Y. Xue, *Electrochim. Acta*, 2014, **146**, 411-418.
16 B. Wang, X. Y. Lu and Y. Y. Tang, *J. Mater. Chem. A*, 2015, **3**, 9689-9699.
17 X. Wang, X. Wu, Y. Guo, Y. Zhong, X. Cao, Y. Ma and J. Yao, *Adv. Funct. Mater.*, 2010, **20**, 1680-1686.
18 L. Zhou, H. Y. Xu, H. W. Zhang, J. Yang, S. B. Hartono, K. Qian, J. Zou and C. Z. Yu, *Chem. Commun.*, 2013, **49**, 8695-8697.
19 Z. Y. Wang, J. S. Chen, T. Zhu, S. Madhavi and X. W. Lou, *Chem.Commun.*, 2010, 4**6**, 6906-6908.
20 G. Y. Zhao, N. Q. Zhang and K. N. Sun, *J. Mater. Chem. A*, 2013, **1**, 221-224.
21 G. Y. Huang, S. M. Xu, S. S. Lu, L. Y. Li and H. Y. Sun, *ACS Appl. Mater. Interfaces*, 2014, **6**, 7236-7243.
22 Y. Wang, F. Yan, S. W. Liu, A. Y. S. Tan, H. H. Song, X. W. Sun and H. Y. Yang, *J. Mater. Chem. A*, 2013, **1**, 5212-5216.
23 S. L. Xiong, J. S. Chen, X. W. Lou and H. C. Zeng, *Adv. Funct. Mater.*, 2012, **22**, 861-871.
24 J. Chen, T. Zhu, Q. Hu, J. Gao, F. Su, S. Qiao and X. Lou, *ACS Appl. Mater. Interfaces*, 2010, **2**, 3628-3635.
25 T. Yang, Y. G. Liu, Z. H. Huang, Q. Yang, M. Guan, M. H. Fang and X. W. Wu, *RSC Adv.*, 2015, **5**, 24486-24493.
26 L. Yu, H. B. Wu and X. W. Lou, *Adv. Mater.*, 2013, **25**, 2296-2300.
27 L. F. Shen, L. Yu, X. Y. Yu, X. G. Zhang and X. W. Lou, *Angew. Chem. Int. Ed.*, 2015, **54**, 1868-1872.
28 L. Zhou, D. Y. Zhao and X. W. Lou, *Adv. Mater.*, 2012, **24**, 745-748.
29 D. L. Wang, Y. C. Yu, H. He, J. Wang, W. D. Zhou and H. D. Abruna, *ACS Nano*, 2015, **9**, 1775-1781.
30 L. Y. Guo, Q. R, X Song, S. J. Hu and Y. D. Mo, *J. Mater. Chem. A*, 2015, **3**, 8683-8692.
31 T. Y. Wei, C. H. Chen, H. C. Chien, S. Y. Lu and C. C. Hu, *Adv. Mater.*, 2010, **22**, 347-351.
32 J. F. Li, S. L. Xiong, X. W. Li and Y. T. Qian, *Nanoscale*, 2013, **5**, 2045-2054.
33 Y. Q. Zhu, C. B. Cao, J. T. Zhang and X. Y. Xu, *J. Mater. Chem. A*, 2015, **3**, 9556-9564.
34 Y. Sharma, N. Sharma, G. Rao and B. Chowdari, *Adv. Funct. Mater.*, 2007, **17**, 2855-2861.
35 D. V. Bavykin, J. M. Friedrich and F. C. Walsh, *Adv. Mater.*, 2006, **18**, 2807-2824.
36 L. L. Hu, B. H. Qu, C. C. Li, Y. J. Chen, L. Mei, D. N. Lei, L. B. Chen, Q. H. Li and T. H. Wang, *J. Mater. Chem. A*, 2013, **1**, 5596-5602.
37 J. Xu, L. Li, P. Gao, L. Yu, Y. J. Chen, P. Yang, S. L. Gai and P. P. Yang, *Electrochim. Acta*, 2015, **166**, 206-214.
38 N. T. Khoa, S. W. Kim, D. V. Thuan, D. H. Yoo, E. J. Kim and S. H. Hahn, *CrystEngComm*, 2014, **16**, 1344-1350.
39 Y. Liu, X. G. Zhang and Y. Wu, *Mater. Chem. Phys.*, 2011, **128**, 475-482.
40 L. Ge, X. Y. Jing, J. Wang, J. Wang, S. Jamil, Q. Liu, F. C. Liu and M. L. Zhang, *J. Mater. Chem.*, 2011, **21**, 10750-10754.
41 Y. F. Zhu, D. H. Fan and W. Z. Shen, *J. Phys. Chem. C*, 2007, **111**, 18629-18635.
42 X. H. Xia, J. P. Tu, J. Zhang, X. H. Huang, X. L. Wang and X. B. Zhao, *Electrochim. Acta*, 2010, **55**, 989-994.
43 W. Zhou, J. Zhang, T. Xue, D. Zhao and H. Li, *J. Mater. Chem.*, 2008, **18**, 905-910.
44 F. Wang, C. C. Lu, Y. F. Qin, C. C. Liang, M. S. Zhao, S. C. Yang, Z. B. Sun and X. P. Song, *J. Power Source*, 2013, **235**, 67-73.
45 Q. S. Xie, D. Q. Zeng, Y. Y. Ma, L. Lin, L. S. Wang and D. L. Peng, *Electrochim. Acta*, 2015, **169**, 283-290.
46 H. Long, T. L. Shi, S. L. Jiang, S. Xi, R. Chen, S. Y. Liu, G. L. Liao and Z. R. Tang, *J. Mater. Chem. A*, 2014, **2**, 3741-3748.
47 W. L. Yao, J. Yang, J. L. Wang and Y. N. Li, J. *Electrochem. Soc.*, 2008, **155**, A903-A908.
48 L. Li, K. H. Seng, Z. X. Chen, Z. P. Guo and H. K. Liu, *Nanoscale*, 2013, **5**, 1922-1928.
49 J. M. Xu, L. He, W. Xu, H. B. Tang, H. Liu, T. Han, C. J. Zhang and Y. H. Zhang, *Electrochim. Acta*, 2014, **145**, 185-192.
50 L. A. Riley, S. H. Lee, L. Gedvilias and A. C. Dillon, *J. Power Sources*, 2010, **195**, 588-592.
51 J. B. Wu, R. Q. Guo, X. H. Huang and Y. Lin, *J. Power Sources*, 2014, **248**, 115-121.

52 J. Y. Wang, N. L. Yang, H. J. Tang, Z. H. Dong, Q. Jin, M. Yang, D. Kisailus, H. J. Zhao, Z. Y. Tang and D. Wang, *Angew. Chem.*, 2013, **125**, 6545-6548.
53 S. Q. Chen, Y. F. Zhao, B. Sun, Z. M. Ao, X. Q. Xie, Y. Y. Wei and G. X. Wang, *ACS Appl. Mater. Interfaces*, 2015, **7**, 3306-3313.
54 W. S. Kim, Y. Hwa, H. C. Kim, J. H. Choi, H. J. Sohn and S. H. Hong, *Nano Res.*, 2014, **7(8)**, 1128-1136.
55 S. H. Choi and Y. C. Kang, *ChemSusChem*, 2013, **6**, 2111-2116.
56 S. G. Mohamed, T. F. Hung, C. J. Chen, C. K. Chen, S. F. Hu, R. S. Liu, K. C. Wang, X. K. Xing, H. M. Liu, A. S. Liu, M. H. Hsiehe and B. J. Leee, *RSC Adv.*, 2013, **3**, 20143-20149.
57 R. R. Wu, X. K. Qian, K. Zhou, J. Wei, J. Lou and P. M. Ajayan, *ACS Nano*, 2014, **8(6)**, 6297-6303.
58 J. Bai, X. G. Li, G. Z. Liu, Y. T. Qian and S. L. Xiong, *Adv. Funct. Mater.*, 2014, **24**, 3012-3020.
59 B. Liu, J. Zhang, X. F. Wang, G. Chen, D. Chen, C. W. Zhou and G. Z. Shen, *Nano Lett.*, 2012, **12**, 3005-3011.
60 T. Yang, Y. G. Liu, Z. H. Huang, Q. Yang, M. Guan, M. H. Fang and X. W. Wu, *RSC Adv.*, 2015, **5**, 24486-24493.
61 L. Y. Guo, Q. Ru, X. Song, S. J. Hu and Y. D. Mo, *RSC Adv.*, 2015, **5**, 19241-19247.
62 N. Du, Y. F. Xu, H. Zhang, J. X. Yu, C. X. Zhai and D. R. Yang, *Inorg. Chem.*, 2011, **50**, 3320-3324.
63 Y. C. Qiu, S. H. Yang, H. Deng, L. M. Jin and W. S. Li, *J. Mater. Chem.*, 2010, **20**, 4439-4444.
64 K. Dewangan, N. N. Sinha, P. K. Sharma, A. C. Pandey, N. Munichandraiah and N. S. Gajbhiye, *CrystEngComm*, 2011, **13**, 927-933.
65 L. Zhou, L. C. Yang, P. Yuan, J. Zou, Y. P. Wu and C. Z. Yu, *J. Phys. Chem. C*, 2010, **114**, 21868-21872.
66 F. Y. Cheng, J. Liang, Z. L. Tao and J. Chen, *Adv. Mater.*, 2011, **23**, 1695-1715.
67 H. Ren, R. B. Yu, J. Y. Wang, Q. Jin, M. Yang, D. Mao, D. Kisailus, H. J. Zhao and D. Wang, *Nano Lett.*, 2014, **14**, 6679-6684.
68 J. Maier, *Phys. Chem. Chem. Phys.*, 2009, **11**, 3011-3022.
69 C. T. Cherian, M. V. Reddy, S. Haur and B. V. R. Chowdari, *ACS Appl. Mater. Interfaces*, 2013, **5**, 918-923.

Table of Contents

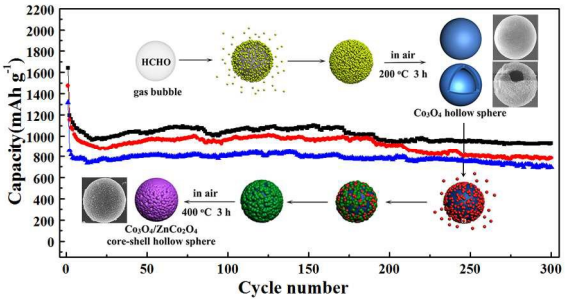

TOC text

Core-shell $Co_3O_4/ZnCo_2O_4$ hollow spheres exhibit superior electrochemical performance with high reversible capacity, excellent cycling stability and good rate capability.